

Article

In-Situ Study of Temperature- and Magnetic-Field-Induced Incomplete Martensitic Transformation in Fe-Mn-Ga

Xiaoming Sun ^{1,2,*}, Jingyi Cui ^{1,2}, Shaofu Li ^{1,2}, Zhiyuan Ma ^{3,4}, Klaus-Dieter Liss ^{5,6}, Runguang Li ⁷ 
and Zhen Chen ^{8,*} 

¹ State Key Laboratory of Multiphase Complex Systems, Institute of Process Engineering, Chinese Academy of Sciences, Beijing 100190, China

² School of Chemical Engineering, University of Chinese Academy of Sciences, Beijing 100049, China

³ Department of Materials Science and Engineering, China University of Petroleum-Beijing, Beijing 102249, China

⁴ X-ray Science Division, Argonne National Laboratory, Argonne, IL 60439, USA

⁵ School of Mechanical, Materials, Mechatronics and Biomedical Engineering, University of Wollongong, Wollongong, NSW 2522, Australia

⁶ Australian Nuclear Science and Technology Organisation, Lucas Heights, NSW 2234, Australia

⁷ Department of Civil and Mechanical Engineering, Technical University of Denmark, DK-2800 Kgs. Lyngby, Denmark

⁸ Xi'an Rare Metal Materials Institute Co., Ltd., Xi'an 710000, China

* Correspondence: xmsun19@ipe.ac.cn (X.S.); cz0521shu@126.com (Z.C.)

Abstract: Significant interest in the stoichiometric and off-stoichiometric Fe₂MnGa alloys is based on their complex phase transition behavior and potential application. In this study, temperature- and magnetic-field-induced phase transformations in the Fe_{41.5}Mn₂₈Ga_{30.5} magnetic shape memory alloy were investigated by in situ synchrotron high-energy X-ray diffraction and in situ neutron diffraction techniques. It was found that incomplete phase transformation and phase coexistence behavior are always observed while applying and removing fields in Fe_{41.5}Mn₂₈Ga_{30.5}. Typically, even at 4 K and under 0 T, or increasing the magnetic field to 11 T at 250 K, it can be directly detected that the martensite and austenite are in competition, making the phase transition incomplete. TEM observations at 300 K and 150 K indicate that the anti-phase boundaries and B2 precipitates may lead to field-induced incomplete phase transformation behavior collectively. The present study may enrich the understanding of field-induced martensitic transformation in the Fe-Mn-Ga magnetic shape memory alloys.

Keywords: magnetic shape memory alloy; martensitic transformation; Fe-Mn-Ga; incomplete phase transformation



Citation: Sun, X.; Cui, J.; Li, S.; Ma, Z.; Liss, K.-D.; Li, R.; Chen, Z. In-Situ Study of Temperature- and Magnetic-Field-Induced Incomplete Martensitic Transformation in Fe-Mn-Ga. *Crystals* **2023**, *13*, 1242. <https://doi.org/10.3390/cryst13081242>

Academic Editor: Vladimir I. Zverev

Received: 25 July 2023

Revised: 7 August 2023

Accepted: 9 August 2023

Published: 11 August 2023



Copyright: © 2023 by the authors. Licensee MDPI, Basel, Switzerland. This article is an open access article distributed under the terms and conditions of the Creative Commons Attribution (CC BY) license (<https://creativecommons.org/licenses/by/4.0/>).

1. Introduction

Ferromagnetic shape memory alloys (FSMAs) have attracted considerable attention due to their multifunctional properties, such as magnetic-field-induced strain [1–4], magnetoresistance [5–7], magnetocaloric effect [8–10], magnetothermal conductivity [11], and exchange bias behavior [12,13]. These properties make them promising materials for applications such as rapid actuators [1], efficient magnetic refrigerators [14], and recording materials [15]. In general, most FSMAs have interesting structural and magnetic properties resulting from their first-order phase transformation induced by external fields [1–13]. Typically, for the Ni-(Co)-Mn-X (X = In, Sn, Sb) alloys, magnetic fields may induce a structural transformation from weak magnetic martensite to ferromagnetic austenite at temperatures close to the austenitic transformation start temperature, leading to some pronounced magnetic-field-induced effects [2–7,16]. Another representative FSMA, i.e., Fe-Mn-Ga alloys displaying distinct and complex magnetic-field-induced martensitic transformation behavior in some out-stoichiometric compositions, are not yet completely understood.

Since Omori et al. reported that the $\text{Fe}_{43}\text{Mn}_{28}\text{Ga}_{29}$ alloy can go through martensitic transition from the paramagnetic (PM) cubic austenite phase to the ferromagnetic (FM) tetragonal martensite phase [17], the search for Fe-Mn-Ga alloys undergoing phase transformations and possessing related multifunctional properties has never stopped. Zhu et al. observed that a magnetic-field-induced transformation from the PM parent phase to the FM martensite phase takes place at 163 K for the slightly off-stoichiometric $\text{Fe}_{50}\text{Mn}_{22.5}\text{Ga}_{27.5}$ alloy, leading to large differences in magnetization between both phases and a huge shape memory strain of up to 3.6% [18]. Researchers found that the martensitic transition in Fe-Mn-Ga alloys can lead to significant changes in their magnetic and optical properties [19–21]. Recently, local symmetry-breaking behavior has been observed in $\text{Fe}_{50}\text{Mn}_{23}\text{Ga}_{27}$, which suppresses the martensitic transition while retaining the magnetic transition in the alloy [22]. In addition, giant exchange bias behavior resulting from the exchange coupling between the coexisting antiferromagnetic (AFM) and FM phase in the Fe-Mn-Ga alloys was achieved, resulting in an enhanced coercivity [23–25]. In the above works, martensitic transformation in Fe-Mn-Ga alloys always displayed significant transformation hysteresis across an incomplete process, which is considered as an obstacle to realize a recoverable and complete field-induced martensitic transformation [26,27]. To some extent, this could limit their applications as, for example, magnetocaloric and magnetostrain materials, and clarifying the mechanism of incomplete phase transformation is essential.

As a result, based on the previous studies, it is essential to carry out an in situ study on the structure and magnetic phase evolution of the Fe-Mn-Ga alloy across martensitic transformation under external fields, such as temperature and magnetic fields. In the present study, we prepared a $\text{Fe}_{41.5}\text{Mn}_{28}\text{Ga}_{30.5}$ alloy presenting martensitic transformation, and the temperature- and magnetic-field-induced phase transformation behaviors of this alloy were systematically studied. The potential reasons for this incomplete phase transformation behavior were discussed, which may be instructive for understanding the underlying mechanisms responsible for the multifunctional properties of Fe-Mn-Ga alloys.

2. Experimental Section

A $\text{Fe}_{41.5}\text{Mn}_{28}\text{Ga}_{30.5}$ magnetic shape memory alloy was prepared by repeated melting in an arc furnace under an argon atmosphere. The rod ingots were sealed in a quartz tube filled with high-purity argon gas, homogenized at 1273 K for 24 h, and finally quenched in cold water. The composition of $\text{Fe}_{41.5}\text{Mn}_{28}\text{Ga}_{28.5}$ was measured using an electron probe microanalyzer (EPMA-1720H, SHIMADZU, Tokyo, Japan). The composition was determined by averaging the compositions of five randomly measured points, and the result was $\text{Fe}_{41.5\pm 0.1}\text{Mn}_{28\pm 0.6}\text{Ga}_{28.5\pm 0.3}$. Due to the fact that Fe-Mn-Ga polycrystalline samples are very brittle, a single crystal with a roughly ellipsoid shape was obtained using the grain growth method [17] by annealing at 1273 K for 168 h, followed by quenching in ice water.

The microstructure was characterized by scanning electron microscopy (SEM, Zeiss Supra 55, Oberkochen, Germany) and transmission electron microscopy (TEM, JEM-2100 F, JEOL, Tokyo, Japan). The phase transition temperatures of the polycrystalline sample and the single crystal sample were analyzed by differential scanning calorimetry (DSC, Netzsch DSC 214 Polyma, Selb, Germany) experiments performed with heating and cooling rates of $10 \text{ K}\cdot\text{min}^{-1}$. The magnetic measurements and electrical resistivity measurements of the polycrystalline samples with sizes of $\Phi 3 \times 1 \text{ mm}^3$ and $10 \times 2 \times 1 \text{ mm}^3$, respectively, were conducted using a physical property measurement system (PPMS, Quantum Design) with a cooling and heating rate of $5 \text{ K}\cdot\text{min}^{-1}$. The external magnetic field is perpendicular to the plane of the polycrystalline sample. The resistivity test was based on a 4-point probe method. The strain, during martensitic transformation for the polycrystalline sample, was performed using a strain gauge glued to the sample and a data logger (TDS102, Tokyo Sokki Kenkyujo Co., Ltd, Tokyo, Japan) under zero field with a cooling and heating rate of $5 \text{ K}\cdot\text{min}^{-1}$. Temperature-dependent in-situ synchrotron high-energy X-ray diffraction

(HEXRD) experiments were carried out at the 11-ID-C beamline at the Advanced Photon Source of Argonne National Laboratory (ANL). A monochromatic X-ray beam with a wavelength of 0.1173 Å was used. The diffraction Debye rings were collected using a two-dimensional (2D) large area detector. The polycrystalline samples were rotated at high speed to obtain full rings and eliminate the effects of preferred orientation during heating and cooling with a rough rate of 3 K·min⁻¹. The samples were cooled and heated in a step-wise manner between 380 K and 119 K, with an average temperature interval of 3 K. At each temperature step, the sample was soaked for five minutes to reach a thermally stabilized state. A small cryogenic detector and an infrared detector were applied during cooling and heating, respectively. Based on the X-ray diffraction intensity theory, the integral intensities of diffraction peaks are proportional to the volume fractions of the corresponding phases. As a result, the volume fractions of the martensite phase (V_M) and austenite phase (V_A) were obtained according to the following expression [28]:

$$V_A = \left(1 + \frac{I_{hkl}^M R_{hkl}^A}{I_{hkl}^A R_{hkl}^M}\right)^{-1} \quad (1)$$

$$V_A + V_B = 1 \quad (2)$$

where I_{hkl}^M and I_{hkl}^A represent the integrated intensities of the considered {hkl} lattice plane, and R_{hkl}^M and R_{hkl}^A are the corresponding theoretical calculated intensities [28]. The crystal structural evolution during the increasing and decreasing of the magnetic fields was studied by in situ neutron diffraction experiments on the high intensity diffractometer WOMBAT [29] at the Australian Nuclear Science and Technology Organisation (ANSTO). The WOMBAT instrument was equipped with a 2D position-sensitive area detector that covered 120° in 2θ on the sample in the diffraction plane and about 15° in the vertical, out-of-plane direction. For the in situ measurements, WOMBAT was equipped with a vertical field magnet (field range of 0 T–11 T with 200 Oe·s⁻¹) with a temperature range of 1.5–300 K (2 K·min⁻¹ during cooling and heating). A polycrystalline sample and a single crystal sample were glued to pure aluminum bolts (where the bolts were used as is) separately for the test under the temperature field and that under the magnetic field. A wavelength of 2.41 Å was used for the measurements.

3. Results and Discussion

The phase transformation temperatures of the Fe_{41.5}Mn₂₈Ga_{30.5} alloy are revealed by the DSC curves in Figure 1a,b. For the polycrystalline sample (Figure 1a), the martensitic transformation and its reverse transformation were revealed by multiple exothermal/endothemic peaks, which are considered to be jerky characteristics of martensitic transformations that have been reported in many alloy systems [30,31]. In contrast, the single-crystal sample showed exothermal/endothemic peaks which are easier to distinguish in Figure 1b, indicating that grain boundaries may play important roles in presenting this “avalanche” behavior during phase transition [30]. M_s , M_f , A_s and A_f in Figure 1b are the martensitic and reverse transformation start and finish temperatures, and they were determined to be about 229 K, 201 K, 298 K, and 329 K, respectively. The temperature dependence of the resistivity $\rho(T)$ for the polycrystalline Fe_{41.5}Mn₂₈Ga_{30.5} is shown in Figure 1c. Fe_{41.5}Mn₂₈Ga_{30.5} showed a significant temperature hysteresis of resistivity on heating and cooling, which indicates a first-order phase transformation in the alloy. One can notice that the transformation temperature interval here was wider than that shown in the DSC results, which may result from the gradual phase transition beyond the peak temperature regions only releasing or absorbing a small fraction of heat that is insufficient to form visible DSC peaks. A significant decrease with a magnetoresistance $\Delta\rho/\rho_{224K}$ ($\Delta\rho = |\rho_{10K} - \rho_{224K}|$) of 8% during cooling can be seen in Fe_{41.5}Mn₂₈Ga_{30.5}, which is ascribed to the forward martensitic transformation. Actually, this is quite different from the temperature dependence of resistivity behavior across martensitic transformation

in most Ni-Mn-based FSMA, where the resistivity usually increases during cooling and decreases during heating [32–35]. Specifically, the electrical resistivity of the austenite phase decreases with the increase in temperature, which is opposite to the austenite phase with metallic behavior in most FSMA, where the electrical resistivity increases with increasing temperatures [36–38]. Figure 1d shows that a remarkable strain up to 0.47% during cooling and heating can be achieved in the polycrystal sample.

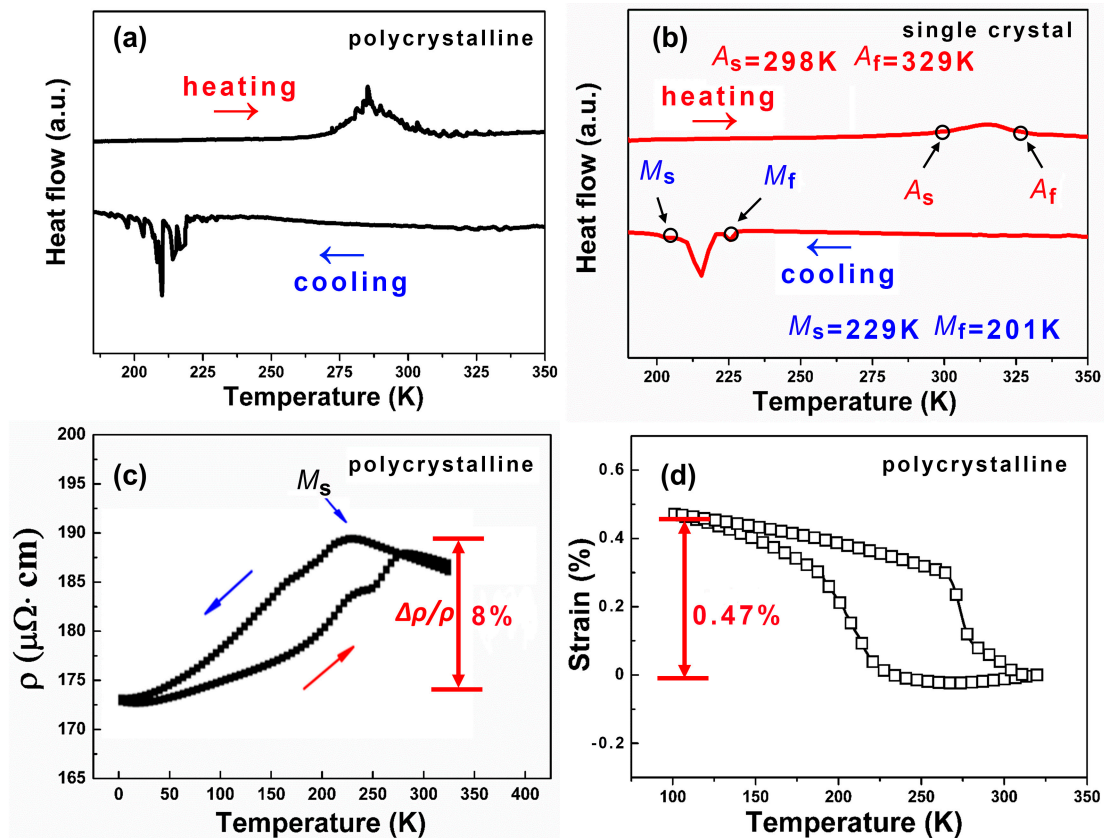


Figure 1. DSC curves for (a) the $\text{Fe}_{41.5}\text{Mn}_{28}\text{Ga}_{30.5}$ polycrystalline sample and (b) the $\text{Fe}_{41.5}\text{Mn}_{28}\text{Ga}_{30.5}$ single-crystal sample. (c) Temperature dependence of electrical resistivity during cooling and heating for polycrystalline $\text{Fe}_{41.5}\text{Mn}_{28}\text{Ga}_{30.5}$. (d) Shape memory effect of polycrystalline $\text{Fe}_{41.5}\text{Mn}_{28}\text{Ga}_{30.5}$, measured without preloading. M_s , M_f , A_s , and A_f in Figure 1b denote the martensitic and reverse transformation starting and finishing temperatures, respectively.

To trace how the structure evolves when temperature changes, the variable-temperature HEXRD patterns for $\text{Fe}_{41.5}\text{Mn}_{28}\text{Ga}_{30.5}$ during the cooling and heating processes are displayed in Figure 2a,b. The results clearly indicate that the samples underwent a structural transformation from the $L2_1$ cubic structure (space group No. 225, $Fm\bar{3}m$) to the tetragonal structure (space group No. 139, $I4/mmm$) during the cooling process. It can be noticed that the competition and coexistence of the two phases are always presented in the whole temperature range during cooling and heating, as indicated by the gradual changes in peak intensities for the two phases. In Figure 2a, at 380 K, the cubic austenite is dominant in the sample, and only a tiny amount of martensite can be observed; a sudden increase in the intensities of tetragonal martensite phase peaks appears when cooling to 238 K. One should notice that there is a discrepancy in the martensitic transformation temperature obtained by DSC (Figure 1a) and HEXRD (here, we all used polycrystalline alloys for comparison), which may result from the different parts of the ingot being used for DSC and HEXRD tests. Different cooling rates may also affect the phase transformation temperatures as determined by two methods. When decreasing the temperature, the intensities of martensite peak continued to increase at the cost of austenite until the sample reached

equilibrium, where both phases were found to be continuously co-existent down to 119 K. The variable-temperature HEXRD patterns for $\text{Fe}_{41.5}\text{Mn}_{28}\text{Ga}_{30.5}$ during heating, shown in Figure 2b, presented a trend nearly opposite to that in Figure 2a, where the intensities of austenite suddenly increased at 271 K. Generally, the lattice volumes of austenite and martensite decrease upon cooling. However, when the martensitic transformation occurs, the phase fraction of martensite increases at the cost of austenite. This can lead to a negative thermal expansion effect in the present alloy [27]. Figure 2c shows that the phase fractions of both phases almost remained unchanged until the temperature decreased to 235 K, where the martensitic transformation started. The austenite phase fraction then decreased from 95% to 25%, while the martensite phase fraction increased from 5% to 75%. Further cooling failed to bring additional obvious changes in phase fractions at temperatures below 140 K, indicating completion of the martensitic transformation. Typically, a large lattice distortion of $(c - a)/a = 32.3\%$ was obtained during the martensitic transformation, where $a = \sqrt{2}a_M = 5.208 \text{ \AA}$ and $c = c_M = 6.891 \text{ \AA}$ were calculated at 238 K from Figure 2a. Such a significant lattice distortion leads to a considerable shape memory effect, as displayed in Figure 1d. To detect the phase compositions at cryogenic temperatures, an in situ neutron diffraction experiment was performed at 4 K, and the results are shown in Figure 2d. One can see that, even at such a low temperature, the two phases still coexisted stably. At 4 K, the transformation was essentially stopped, and the crystal consisted of two phases. Overall, the picture of the martensitic transformation of the average structure in $\text{Fe}_{41.5}\text{Mn}_{28}\text{Ga}_{30.5}$ in this work is nucleation-driven [21], continuous, and incomplete.

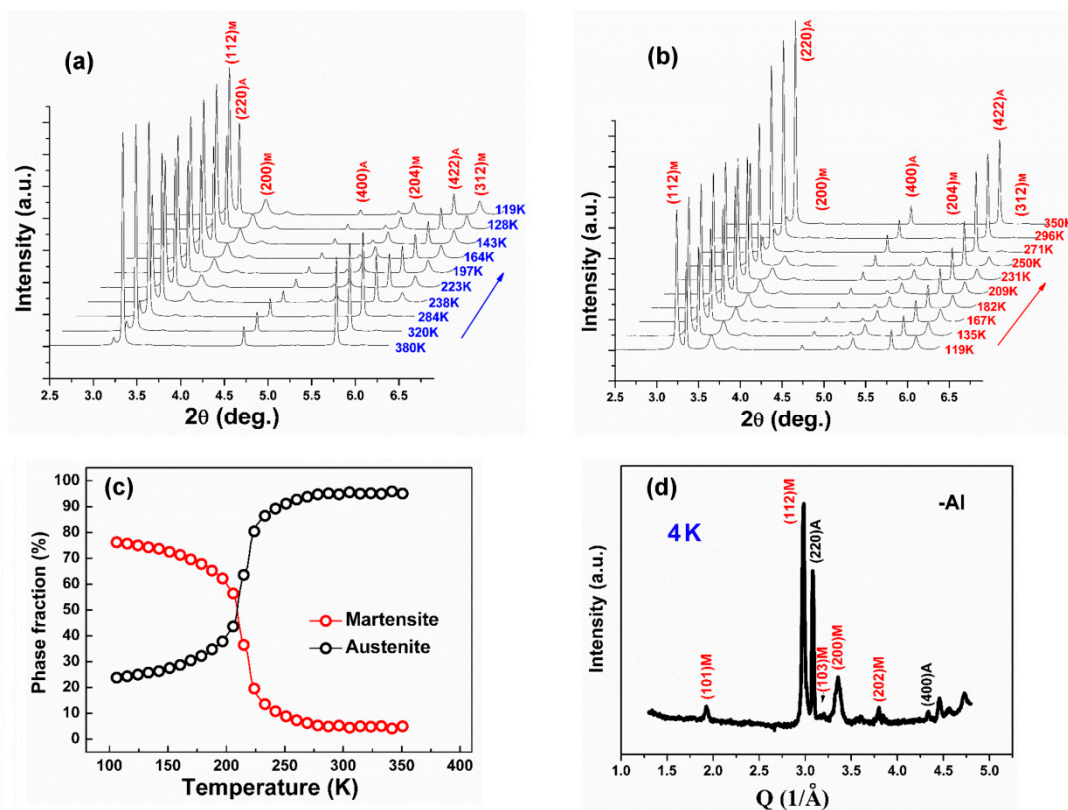


Figure 2. HEXRD patterns measured for the $\text{Fe}_{41.5}\text{Mn}_{28}\text{Ga}_{30.5}$ polycrystalline sample during (a) cooling and (b) heating. (c) Temperature dependence of the phase fractions, as obtained using Equations (1) and (2) during cooling for $\text{Fe}_{41.5}\text{Mn}_{28}\text{Ga}_{30.5}$. (d) One-dimensional (1D) diffraction patterns at 4 K without applying magnetic field for $\text{Fe}_{41.5}\text{Mn}_{28}\text{Ga}_{30.5}$. The letters “A” and “M” in the indices in (a) and (d) denote austenite and martensite, respectively.

The temperature dependence of the phase fraction growth rate data for $\text{Fe}_{41.5}\text{Mn}_{28}\text{Ga}_{30.5}$ (Figure 3) illustrates the hysteresis effect and the broad temperature range of transformation

on both the heating and cooling processes. As shown in Figure 3, at 150 K and 330 K, the martensite and austenite growth rates were essentially below 0.5%, and the martensite and austenite phases accounted for about 75% and 25% of the structure at 150 K, as discussed in Figure 2c; the martensitic transformation was incomplete. The phase fraction growth rates showed two peaks at 213 ± 2 K during cooling and 278 ± 2 K during heating, respectively, further indicating a significant phase transformation hysteresis of 65 K in the $\text{Fe}_{41.5}\text{Mn}_{28}\text{Ga}_{30.5}$ alloy. This phase transformation hysteresis was larger than that shown in Figure 2, which was calculated to be about 33 K. This is because the phase fraction growth rate may be more sensitive in detecting the phase transformation start and stop timestamps.

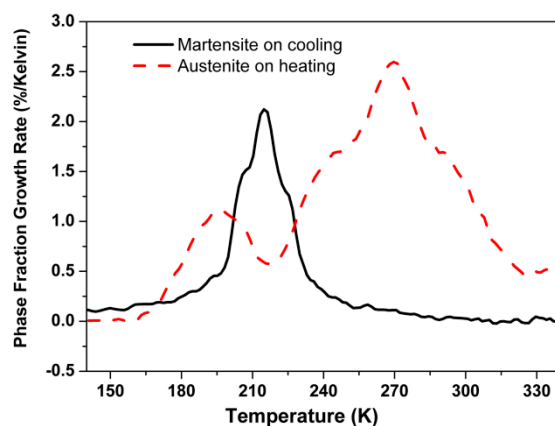


Figure 3. The temperature dependence of the phase fraction growth rate data for polycrystalline $\text{Fe}_{41.5}\text{Mn}_{28}\text{Ga}_{30.5}$.

The thermomagnetization curves ($M(T)$ curves) of $\text{Fe}_{41.5}\text{Mn}_{28}\text{Ga}_{30.5}$ during cooling and heating under magnetic fields of 0.03 T, 0.5 T, and 2 T are shown in Figure 4a. The magnetization increased significantly in certain temperature windows during the first cooling under 0.03 T, corresponding to the martensitic transformation, and significantly decreased in the magnetization during heating, with a result of under 0.03 T due to the reverse martensitic transformation. One can notice from the $M(T)$ curves that the martensite and austenite are considered to be ferromagnetic and paramagnetic, respectively [17]. When applying a magnetic field of 0.5 T, a large ΔM increased across martensitic transformation. Such a relatively large ΔM raised the transformation temperatures as compared to the phase transformation temperatures under 0.03 T. When it came to 2 T, ΔM became larger, and the phase transformation temperatures shifted towards higher temperatures. Usually, in the Ni-Mn-based FSMAs, the shift of the transformation temperatures under high magnetic fields is towards lower temperature areas compared with that under low magnetic fields [39–43]. However, the direction of the shift of phase transformation temperature under magnetic fields in Fe-Mn-Ga alloys was reversed. The difference in the magnetism of austenite and martensite could account for the abnormal shifting direction in Fe-Mn-Ga. Figure 4b shows the magnetization curves at different temperatures during cooling ($M(H)$ curves) for $\text{Fe}_{41.5}\text{Mn}_{28}\text{Ga}_{30.5}$. The austenite remained in the paramagnetism at 380 K, but still showed apparent magnetization behavior, which is caused by the residual martensite. The $M(H)$ curve showed quite significant hysteresis between the field-up and field-down at 250 K, 210 K, 130 K, and 60 K (taken one after the other), indicating a magnetic field-induced transformation within a wide temperature range in this alloy system. When the temperature was decreased to 4 K, the curve exhibited typical ferromagnetic properties [17]. The saturate magnetization of the martensite was estimated to be $72 \text{ emu} \cdot \text{g}^{-1}$ at 4 K. Notably, the magnetic-field-induced transformation in the present alloy occurred from the paramagnetic austenite phase to the ferromagnetic martensitic phase, which is also the opposite of that of most other FSMAs [44–47]. This is caused when the martensitic transformation scuffles with the spontaneous magnetization transition in this sample [18]. Figure 4c shows the saturation magnetization as a function of the various temperatures at

which the $M(H)$ loops were taken. One can see that the saturation magnetization values presented a sharp increase from 250 K and 130 K, and then remained unchanged during further cooling.

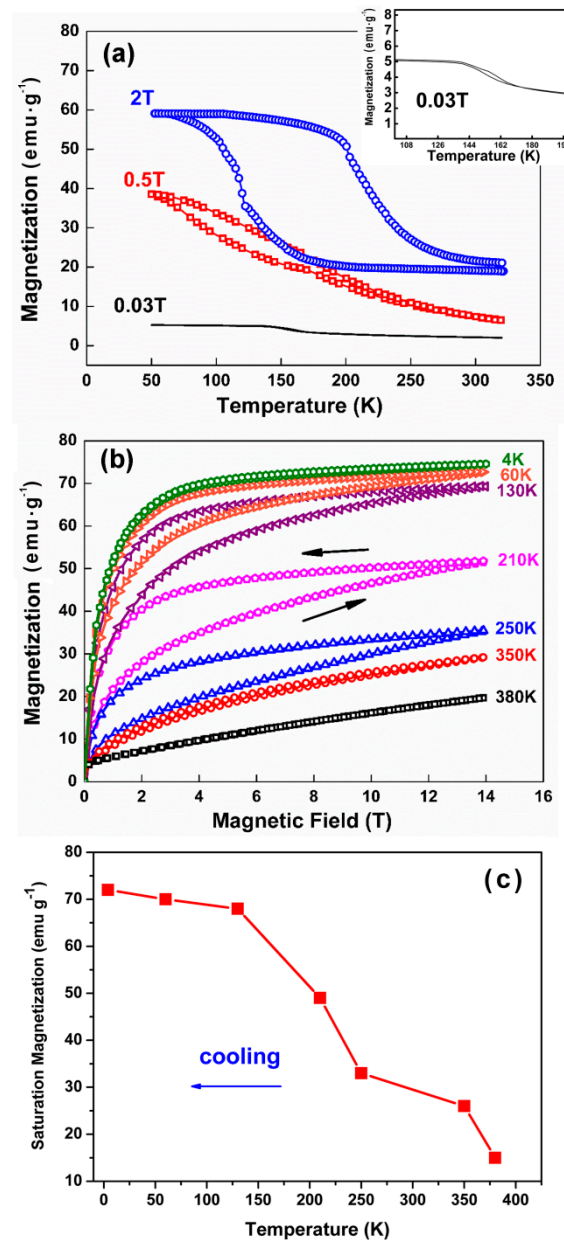


Figure 4. (a) Magnetization under 0.03 T, 0.5 T, and 2 T [$M(T)$] during cooling and heating for polycrystalline $\text{Fe}_{41.5}\text{Mn}_{28}\text{Ga}_{30.5}$, respectively. The inset shows the enlarged $M(T)$ curve of 0.03 T. (b) Isothermal magnetization [$M(H)$] curves were recorded at 380 K, 350 K, 250 K, 210 K, 130 K, 60 K and 4 K for polycrystalline $\text{Fe}_{41.5}\text{Mn}_{28}\text{Ga}_{30.5}$. (c) The saturation magnetization as a function of the various temperatures at which the M-H loops were taken.

To trace how the structure develops under magnetic fields, in situ neutron diffraction experiments were further used to monitor the structural evolution along with increasing and decreasing magnetic fields in a $\text{Fe}_{41.5}\text{Mn}_{28}\text{Ga}_{30.5}$ single-crystal alloy. For the in situ neutron diffraction experiments, the sample was first cooled from 400 K (furnace) to 250 K, and then at 250 K, reciprocal space mapping was presented along with increasing and decreasing magnetic fields in the sequence of 0 T–2 T–6 T–11 T–0 T (field ramped from 0 to 2 T, then measurement was performed, then it was ramped to 6 T and the 2nd measurement

was performed, etc.). The reciprocal space maps measured at different magnetic fields are shown in Figure 5a–d. The coordinates of these figures are expressed with respect to the scattering vector \mathbf{Q} with the length $Q = 2\pi/d = 4\pi \sin \theta / \lambda$, with d being the interplanar spacing and 2θ the diffraction angle. One-dimensional (1D) diffraction patterns from azimuthal integration of the reciprocal space maps in the Q range from 2.0 \AA^{-1} to 4.0 \AA^{-1} with the increasing and decreasing magnetic fields are shown in Figure 5e. The reciprocal space map shown in Figure 5a indicates that, at 250 K, the sample was in the austenite state, and all the diffraction spots were well indexed according to the $L2_1$ cubic structure with lattice parameter $a = 5.675 \text{ \AA}$. The two continuous diffraction rings in Figure 5a stem from the reflections of the polycrystalline aluminum bolt to which the sample was glued. One can see from Figure 5b that for $\text{Fe}_{41.5}\text{Mn}_{28}\text{Ga}_{30.5}$ under the magnetic field of 2 T, no obvious change in the diffraction patterns could be observed, and only the diffraction spot of $(220)_A$ (A denotes austenite) could be detected. In contrast, when the field was increased to 11 T (Figure 5c), diffraction patterns of martensite appeared [$(112)_M$ and $(200)_M$], while the intensity of the diffraction pattern for austenite significantly decreased. This process corresponds well to the $M(H)$ curve at 250 K in Figure 4b. It should be noted that under 11 T, and even decreasing the field to 0 T (Figure 5d), both the transformation from austenite to martensite and its recovery transition were still incomplete. This could be attributed to the significant hysteresis in the Fe-Mn-Ga alloy system, and this will be discussed later.

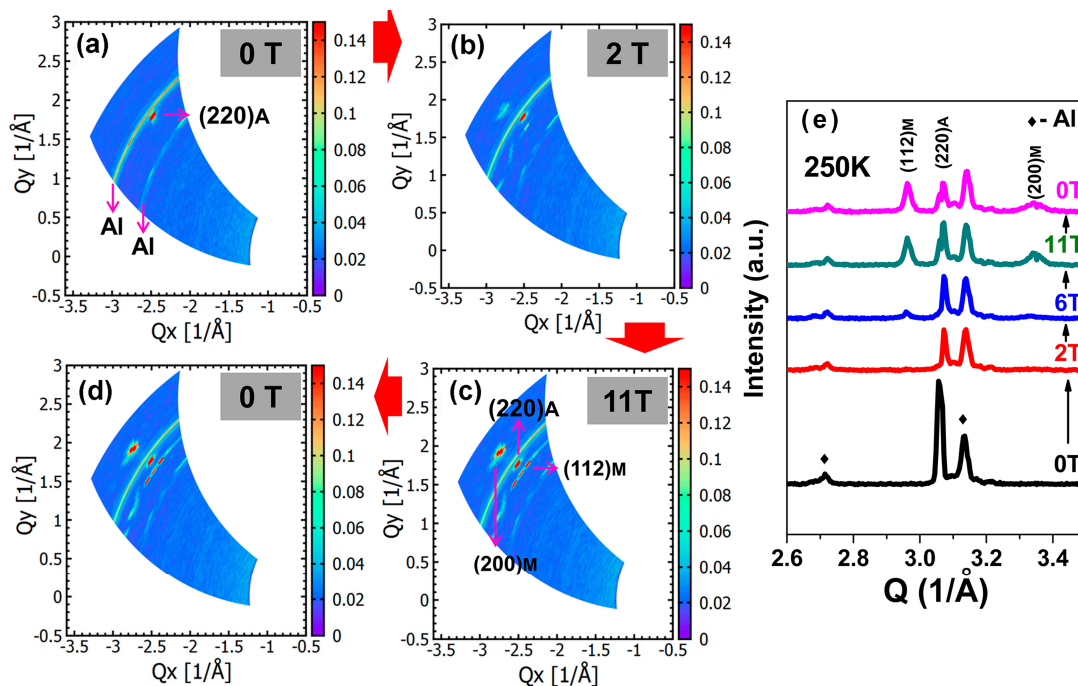


Figure 5. Reciprocal space maps measured at 250 K for the polycrystalline $\text{Fe}_{41.5}\text{Mn}_{28}\text{Ga}_{30.5}$ alloy with a magnetic field increasing from (a) 0 T to (b) 2 T and (c) 11 T, and then with a magnetic field decreasing to (d) 0 T; (e) 1D diffraction patterns, obtained by azimuthal integration of the reciprocal space maps (in the Q range from 2.0 \AA^{-1} to 4.0 \AA^{-1}), for different magnetic field values at 250 K.

Figure 6a shows the evolution of the intensity ratios of the specific diffraction spots of martensite and austenite, namely, $I(112)_M/I(220)_A$ and $I(200)_M/I(220)_A$, with increasing and decreasing magnetic fields in the $\text{Fe}_{41.5}\text{Mn}_{28}\text{Ga}_{30.5}$ alloy at 250 K. One can see that there was no obvious change in the intensity ratios $I(112)_M/I(220)_A$ and $I(200)_M/I(220)_A$ when the magnetic field changed from 0 T to 2 T and 6 T. Strikingly, there was a sharp increase in the intensity ratios $I(112)_M/I(220)_A$ and $I(200)_M/I(220)_A$ when the magnetic field increased to 11 T, as seen from Figure 6a. These results indicate that the volume fraction of martensite became higher, as is consistent with the increase in magnetization from 0 T to 11 T on the $M(H)$ curve at 250 K. When the magnetic field was removed,

the intensity ratios $I(112)_M/I(220)_A$ and $I(200)_M/I(220)_A$ almost remained unchanged, indicating the incomplete recovery transition. Figure 6b shows the evolution of lattice parameters for martensite and austenite with the increasing and decreasing magnetic field. With the increasing and decreasing magnetic field, the lattice parameters for martensite and austenite only presented slight changes when martensitic transformation and its reverse transformation occurred, indicating that at 250 K, the magnetic field was unable to provide sufficient energy to easily overcome atomic connection energies to vary both phases' lattice parameters, although partial austenite still continued transforming into martensite. An abrupt unit cell volume increase, i.e., $\Delta V/V = +1.29\%$, could be achieved when increasing the magnetic field to 2 T, which is very close to that reported previously [17,18].

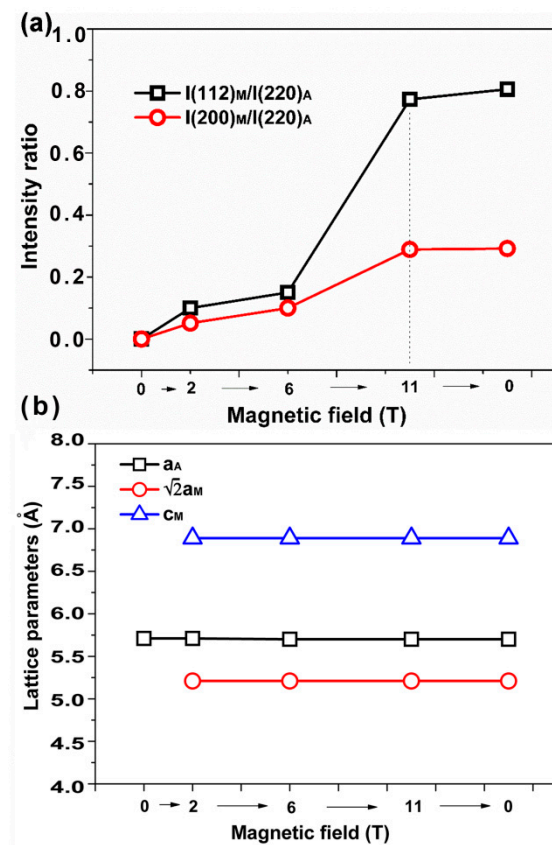


Figure 6. (a) Evolution of the intensity ratios, $I(112)_M/I(220)_A$ and $I(200)_M/I(220)_A$, as a function of magnetic field at 250 K. (b) Evolution of lattice parameters for $\text{Fe}_{41.5}\text{Mn}_{28}\text{Ga}_{30.5}$ as a function of magnetic field at 250 K.

Since the temperature- and magnetic-field-induced incomplete phase transformation behaviors in the $\text{Fe}_{41.5}\text{Mn}_{28}\text{Ga}_{30.5}$ alloy were systematically studied by means of in situ experiments, a further microstructural analysis by TEM is shown in Figure 7. Figure 7a presents a TEM image for $\text{Fe}_{41.5}\text{Mn}_{28}\text{Ga}_{30.5}$, taken at 300 K (cooling from 400 K), and Figure 7b shows an enlarged view of a local area in Figure 7a. No obvious characteristic morphology of martensite-like minor long strip-type grain can be seen in Figure 7a. Instead, some anti-phase boundaries [48] (APBs, marked by red arrows in Figure 7a) can be detected. The APBs' thickness was around 20–40 nm, and it was reported that in the Fe-Mn-Ga alloys, the APBs' crystal structure may appear while changing from $L2_1$ to lower-ordered B2 phases by quenching (B2 shares the same fundamental spots with $L2_1$) [28]. The corresponding selected area diffraction patterns of Figure 7a are shown in Figure 7a', confirming the present area to be the $L2_1$ austenite phase state. In addition, some weak reflections, which may come from a lower-ordered B2 phase, appear at the positions between the austenite spots, as indicated with the red arrow in Figure 7a', which represents

the precipitates. Similar precipitates were found previously by Omori et al. [49] in Fe-Mn-Al alloys. It is reported that in the classical Fe-Ga alloy systems, the cubic-to-tetragonal phase transformation can develop within the B2 precipitates, leading to the multidomain structure being confined within a fixed-shape particle and to an incomplete transformation [50]. A similar episode could have occurred during the martensitic transformation process in Fe-Mn-Ga for the present work. When the sample was cooled to 150 K, as shown in Figure 7c, some long strip-type grains could be seen, some of which referred to the martensite. The width of the long strip-type grain was about 70 nm, as measured in Figure 7d. The corresponding selected area diffraction patterns of Figure 7c are shown in Figure 7c', and one can see that, except for the L2₁ austenite phase (body-centered-cubic, bcc), some reflections can be identified as variants of [112] martensite (body-centered-tetragonal, bct), while the ordered B2 precipitates with {100} superlattice reflection spots can be detected within in the matrix along the [011] zone axis.

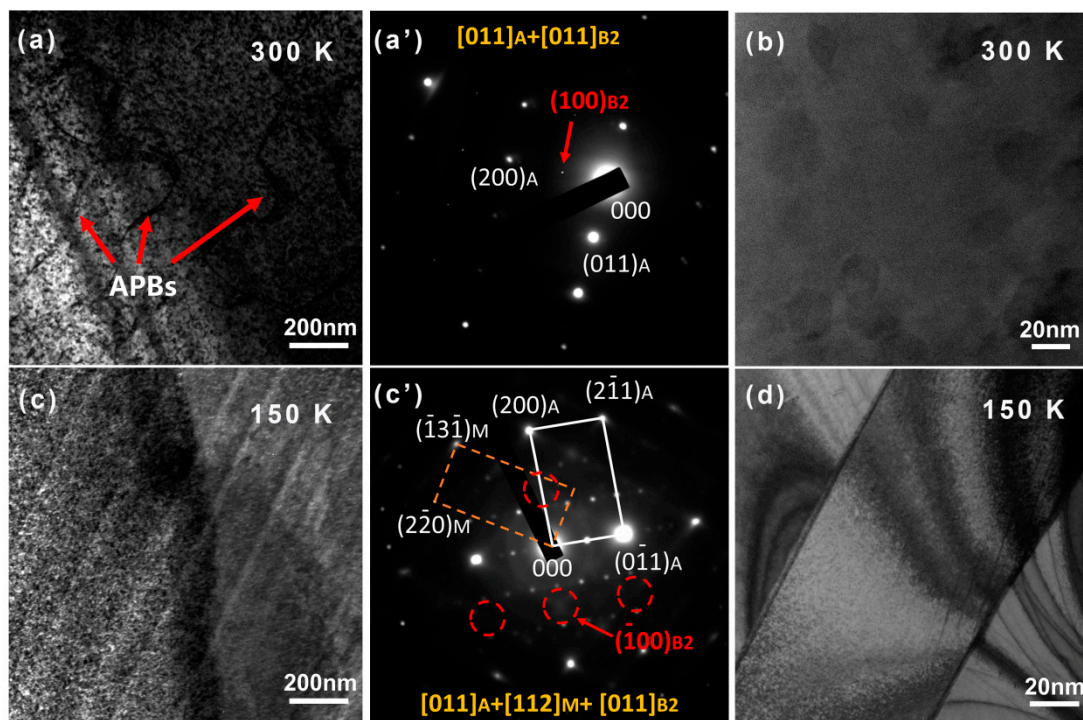


Figure 7. TEM observations of the $\text{Fe}_{41.5}\text{Mn}_{28}\text{Ga}_{30.5}$ alloy at (a) 300 K and (c) 150 K, with the selected area diffraction patterns at these temperatures shown in (a',c'), respectively. (b,d) are two enlarged views of a local area in in (b,c), respectively.

In the present work, the existence of APBs was able to weaken the degree of local ordering, further leading to a decrease in the kinetics during martensitic transformation and an increase in internal stress around APBs to inhibit the subsequent development of martensitic transformation. Furthermore, the existence of B2 precipitates and their nucleation may only result from the vacancy absorption [51]. As precipitates, they may be formed by certain element enrichment of the Fe-Mn-Ga alloy, leading to a difference in their unit cell volume and an increase in local stress. In this case, precipitation is possible only if the absorbed excess vacancies annihilate this extra volume and, thus, eliminate the transformation-induced stress preventing decomposition. To some extent, the field-induced martensitic transformation of the L2₁ phase is restricted by the ordered B2 phase, either in the actual sample space or characterized by the reciprocal space. This incomplete martensitic transformation can also be discussed from a geometric compatibility (measured by the middle eigenvalue λ_2 of the transformation stretch matrix \mathbf{U}) point of view [52,53], and the middle eigenvalue λ_2 for the Fe-Mn-Ga alloys usually seriously deviates from the perfect geometric compatibility of $\lambda_2 = 1$ [54]. This indicates that the present alloy with

$\lambda_2 = 0.92$ has poor geometric compatibility between austenite and martensite, making the phase transformation between the two phases difficult. The above combined factors collectively affect the temperature- and magnetic-field-induced incomplete phase transformation behaviors of the Fe_{41.5}Mn₂₈Ga_{30.5} alloy.

4. Conclusions

In this work, the temperature- and magnetic-field-induced incomplete martensitic transformation of the Fe_{41.5}Mn₂₈Ga_{30.5} magnetic shape memory alloy was systematically investigated. The temperature-field-induced incomplete phase transformation was directly evidenced by the crystal structure evolution during cooling and heating using the in situ synchrotron high-energy X-ray diffraction technique. The magnetic-field-induced phase transformation was revealed by the crystal structure evolution while increasing and decreasing the magnetic fields by means of in situ neutron diffraction experiments. The results show that even at 4 K, the alloy still presented a two-phase coexistence state. When changing the magnetic fields at 250 K, the phase transformation, which is always accompanied by the competing between martensite and austenite, cannot be accomplished. The variation in the magnitude of the applied magnetic field leads to an irreversible effect of changing the phase composition. TEM observation indicates that the existence of anti-phase boundaries and B2 precipitates may lead to difficulties during field-induced phase transformation. This work may help us to understanding the complex phase transition under external fields in Fe-Mn-Ga alloy systems, and may provide suggestions for the development of applicable Fe-Mn-Ga magnetic shape memory alloys with novel functionalities.

Author Contributions: Conceptualization, X.S. and Z.C.; methodology, K.-D.L.; software, R.L.; validation, Z.M.; formal analysis, R.L. and Z.M.; investigation, X.S. and J.C.; resources, X.S. and S.L.; data curation, X.S. and S.L.; writing—original draft preparation, X.S. and Z.C.; writing—review and editing, X.S. and Z.C.; visualization, X.S.; supervision, X.S. and Z.C.; project administration, X.S.; funding acquisition, X.S. All authors have read and agreed to the published version of the manuscript.

Funding: This research was funded by the National Natural Science Foundation of China (Nos. 52101237 and 52201020).

Data Availability Statement: Not applicable.

Acknowledgments: Gene Davidson and Richard Spence are gratefully acknowledged for their technical support on the sample environments in ANSTO and ANL. We are grateful to Dennis E. Brown for his valuable discussions.

Conflicts of Interest: The authors declare no conflict of interest.

References

1. Ullakko, K.; Huang, J.K.; Kantner, C.; O’handley, R.C.; Kokorin, V.V. Large magnetic-field-induced strains in Ni₂MnGa single crystals. *Appl. Phys. Lett.* **1996**, *69*, 1966. [[CrossRef](#)]
2. Kainuma, R.; Imano, Y.; Ito, W.; Sutou, Y.; Morito, H.; Okamoto, S.; Kitakami, O.; Oikawa, K.; Fujita, A.; Kanomata, T.; et al. Magnetic-field-induced shape recovery by reverse phase transformation. *Nature* **2006**, *439*, 957–960. [[CrossRef](#)]
3. Saren, A.; Laitinen, V.; Vinogradova, M.; Ullakko, K. Twin boundary mobility in additive manufactured magnetic shape memory alloy 10M Ni-Mn-Ga. *Acta Mater.* **2023**, *246*, 118666. [[CrossRef](#)]
4. Krenke, T.; Duman, E.; Acet, M.; Wassermann, E.F.; Moya, X.; Mañosa, L.; Planes, A.; Suard, E.; Ouladdiaf, B. Magnetic superelasticity and inverse magnetocaloric effect in Ni-Mn-In. *Phys. Rev. B* **2007**, *75*, 104414. [[CrossRef](#)]
5. Bachaga, T.; Zhang, J.; Khitouni, M.; Sunol, J.J. NiMn-based Heusler magnetic shape memory alloys: A review. *Int. J. Adv. Manuf. Technol.* **2019**, *103*, 2761–2772. [[CrossRef](#)]
6. Koyama, K.; Okada, H.; Watanabe, K.; Kanomata, T.; Kainuma, R.; Ito, W.; Oikawa, K.; Ishida, K. Observation of large magnetoresistance of magnetic Heusler alloy Ni₅₀Mn₃₆Sn₁₄ in high magnetic fields. *Appl. Phys. Lett.* **2006**, *89*, 182510. [[CrossRef](#)]
7. Yu, S.Y.; Ma, L.; Liu, G.D.; Liu, Z.H.; Chen, J.L.; Cao, Z.X.; Wu, G.H.; Zhang, B.; Zhang, X.X. Magnetic field-induced martensitic transformation and large magnetoresistance in NiCoMnSb alloys. *Appl. Phys. Lett.* **2007**, *90*, 242501. [[CrossRef](#)]
8. Yang, J.; Li, Z.; Yang, B.; Yan, H.; Cong, D.; Zhao, X.; Zuo, L. Strain manipulation of magnetocaloric effect in a Ni_{39.5}Co_{8.5}Mn₄₂Sn₁₀ melt-spun ribbon. *Scr. Mater.* **2023**, *224*, 115141. [[CrossRef](#)]
9. Khan, M.; Ali, N.; Stadler, S. Inverse magnetocaloric effect in ferromagnetic Ni₅₀Mn_{37+x}Sb_{13-x} Heusler alloys. *J. Appl. Phys.* **2007**, *101*, 053919. [[CrossRef](#)]

10. Liu, J.; Gottschall, T.; Skokov, K.P.; Moore, J.D.; Gutfleisch, O. Giant magnetocaloric effect driven by structural transitions. *Nat. Mater.* **2012**, *11*, 620–626. [[CrossRef](#)]
11. Zhang, B.; Zhang, X.X.; Yu, S.Y.; Chen, J.L.; Cao, Z.X.; Wu, G.H. Giant magnetothermal conductivity in the Ni-Mn-In ferromagnetic shape memory alloys. *Appl. Phys. Lett.* **2007**, *91*, 012510. [[CrossRef](#)]
12. Li, Z.; Jing, C.; Chen, J.; Yuan, S.; Cao, S.; Zhang, J. Observation of exchange bias in the martensitic state of Ni₅₀Mn₃₆Sn₁₄ Heusler alloy. *Appl. Phys. Lett.* **2007**, *91*, 112505. [[CrossRef](#)]
13. Wang, B.M.; Liu, Y.; Ren, P.; Xia, B.; Ruan, K.B.; Yi, J.B.; Ding, J.; Li, X.G.; Wang, L. Large exchange bias after zero-field cooling from an unmagnetized state. *Phys. Rev. Lett.* **2011**, *106*, 077203. [[CrossRef](#)]
14. Liu, J.; Woodcock, T.G.; Scheerbaum, N.; Gutfleisch, O. Influence of annealing on magnetic field-induced structural transformation and magnetocaloric effect in Ni-Mn-In-Co ribbons. *Acta Mater.* **2009**, *57*, 4911–4920. [[CrossRef](#)]
15. Takagishi, M.; Koi, K.; Yoshikawa, M.; Funayama, T.; Iwasaki, H.; Sahashi, M. The applicability of CPP-GMR heads for magnetic recording. *IEEE Trans. Magn.* **2002**, *38*, 2277–2282. [[CrossRef](#)]
16. Cong, D.Y.; Roth, S.; Schultz, L. Magnetic properties and structural transformations in Ni-Co-Mn-Sn multifunctional alloys. *Acta Mater.* **2012**, *60*, 5335–5351. [[CrossRef](#)]
17. Omori, T.; Watanabe, K.; Xu, X.; Umetsu, R.Y.; Kainuma, R.; Ishida, K. Martensitic transformation and magnetic field-induced strain in Fe-Mn-Ga shape memory alloy. *Scr. Mater.* **2011**, *64*, 669–672. [[CrossRef](#)]
18. Zhu, W.; Liu, E.K.; Feng, L.; Tang, X.D.; Chen, J.L.; Wu, G.H.; Liu, H.Y.; Meng, F.B.; Luo, H.Z. Magnetic-field-induced transformation in FeMnGa alloys. *Appl. Phys. Lett.* **2009**, *95*, 222512. [[CrossRef](#)]
19. Yang, H.; Chen, Y.; Bei, H.; dela Cruz, C.R.; Wang, Y.D.; An, K. Annealing effects on the structural and magnetic properties of off-stoichiometric Fe-Mn-Ga ferromagnetic shape memory alloys. *Mater. Des.* **2016**, *104*, 327–332. [[CrossRef](#)]
20. Zhang, Y.J.; Wu, Z.G.; Hou, Z.P.; Liu, Z.H.; Liu, E.K.; Xi, X.K.; Wang, W.H.; Wu, G.H. Magnetic-field-induced transformation and strain in polycrystalline FeMnGa ferromagnetic shape memory alloys with high cold-workability. *Appl. Phys. Lett.* **2021**, *119*, 142402. [[CrossRef](#)]
21. Jenkins, C.A.; Scholl, A.; Kainuma, R.; Elmers, H.J.; Omori, T. Temperature-induced martensite in magnetic shape memory Fe₂MnGa observed by photoemission electron microscopy. *Appl. Phys. Lett.* **2012**, *100*, 032401. [[CrossRef](#)]
22. Ma, T.Y.; Liu, X.L.; Yan, M.; Wu, C.; Ren, S.; Li, H.Y.; Feng, M.X.; Qiu, Z.Y.; Ren, X.B. Suppression of martensitic transformation in Fe₅₀Mn₂₃Ga₂₇ by local symmetry breaking. *Appl. Phys. Lett.* **2015**, *106*, 211903. [[CrossRef](#)]
23. Tang, X.D.; Wang, W.H.; Zhu, W.; Liu, E.K.; Wu, G.H.; Meng, F.B.; Liu, H.Y.; Luo, H.Z. Giant exchange bias based on magnetic transition in γ -Fe₂MnGa melt-spun ribbons. *Appl. Phys. Lett.* **2010**, *97*, 242513. [[CrossRef](#)]
24. Tang, X.D.; Wang, W.H.; Wu, G.H.; Meng, F.B.; Liu, H.Y.; Luo, H.Z. Tuning exchange bias by thermal fluctuation in Fe₅₂Mn₂₃Ga₂₅ melt-spun ribbons. *Appl. Phys. Lett.* **2011**, *99*, 222506. [[CrossRef](#)]
25. Shih, C.W.; Zhao, X.G.; Chang, H.W.; Chang, W.C.; Zhang, Z.D. The phase evolution, magnetic and exchange bias properties in Fe₅₀Mn_{24+x}Ga_{26-x} (x = 0–3) melt-spun ribbons. *J. Alloys Compd.* **2013**, *570*, 14–18. [[CrossRef](#)]
26. Sun, X.M.; Cong, D.Y.; Ren, Y.; Liss, K.-D.; Brown, D.E.; Ma, Z.Y.; Hao, S.J.; Xia, W.X.; Chen, Z.; Ma, L.; et al. Magnetic-field-induced strain-glass-to-martensite transition in a Fe-Mn-Ga alloy. *Acta Mater.* **2020**, *183*, 11. [[CrossRef](#)]
27. Sun, X.M.; Cong, D.Y.; Ren, Y.; Brown, D.E.; Li, R.G.; Li, S.H.; Yang, Z.; Xiong, W.X.; Nie, Z.H.; Wang, L.; et al. Giant negative thermal expansion in Fe-Mn-Ga magnetic shape memory alloys. *Appl. Phys. Lett.* **2018**, *113*, 041903. [[CrossRef](#)]
28. E04 Committee. *Practice for X-ray Determination of Retained Austenite in Steel with Near Random Crystallographic Orientation*; ASTM International: West Conshohocken, PA, USA, 2013.
29. Studer, A.J.; Hagen, M.E.; Noakes, T.J. Wombat: The high-intensity powder diffractometer at the OPAL reactor. *Phys. B Condens. Matter* **2006**, *385*, 1013–1015. [[CrossRef](#)]
30. Gallardo, M.C.; Machado, J.; Romero, F.J.; del Cerro, J.; Salje, E.K.H.; Planes, A.; Vives, E.; Romero, R.; Stipcich, M. Avalanche criticality in the martensitic transition of Cu_{67.64}Zn_{16.71}Al_{15.65} shape-memory alloy: A calorimetric and acoustic emission study. *Phys. Rev. B* **2010**, *81*, 174102. [[CrossRef](#)]
31. Soto-Parra, D.E.; Moya, X.; Mañosa, L.; Flores-Zúñiga, A.H.; Alvarado-Hernández, F.; Ochoa-Gamboa, R.A.; Matutes-Aquino, J.A.; Ríos-Jara, D. Fe and Co selective substitution in Ni₂MnGa: Effect of magnetism on relative phase stability. *Philos. Mag.* **2010**, *90*, 2771–2792. [[CrossRef](#)]
32. Yu, S.Y.; Liu, Z.H.; Liu, G.D.; Chen, J.L.; Cao, Z.X.; Wu, G.H.; Zhang, B.; Zhang, X.X. Large magnetoresistance in single-crystalline Ni₅₀Mn_{50-x}In_x alloys (x = 14–16) upon martensitic transformation. *Appl. Phys. Lett.* **2006**, *89*, 162503. [[CrossRef](#)]
33. Han, Z.D.; Wang, D.H.; Zhang, C.L.; Xuan, H.C.; Zhang, J.R.; Gu, B.X.; Du, Y.W. The phase transitions, magnetocaloric effect, and magnetoresistance in Co doped Ni-Mn-Sb ferromagnetic shape memory alloys. *J. Appl. Phys.* **2008**, *104*, 053906. [[CrossRef](#)]
34. Sun, X.M.; Cong, D.Y.; Li, Z.; Zhang, Y.L.; Chen, Z.; Ren, Y.; Liss, K.-D.; Ma, Z.Y.; Li, R.G.; Qu, Y.H.; et al. Manipulation of magnetostructural transition and realization of prominent multifunctional magnetoresponsive properties in NiCoMnIn alloys. *Phys. Rev. Mater.* **2019**, *3*, 034404. [[CrossRef](#)]
35. Sharma, V.K.; Chattopadhyay, M.K.; Shaeb, K.H.B.; Chouhan, A.; Roy, S.B. Large magnetoresistance in Ni₅₀Mn₃₄In₁₆ alloy. *Appl. Phys. Lett.* **2006**, *89*, 222509. [[CrossRef](#)]
36. Huang, X.M.; Zhao, Y.; Yan, H.L.; Jia, N.; Yang, B.; Li, Z.; Zhang, Y.; Esling, C.; Zhao, X.; Zuo, L. Giant magnetoresistance, magnetostress and magnetocaloric effects in a Cu-doped<001>-textured Ni₄₅Co₅Mn₃₆In_{13.2}Cu_{0.8} polycrystalline allo. *J. Alloys Compd.* **2021**, *889*, 161652.

37. Zheng, T.T.; Liu, K.; Chen, H.X.; Wang, C. Large magnetocaloric and magnetoresistance effects during martensitic transformation in Heusler-type Ni₄₄Co₆Mn₃₇In₁₃ alloy. *J. Magn. Magn. Mater.* **2022**, *563*, 170034. [[CrossRef](#)]
38. Huang, L.; Cong, D.Y.; Ma, L.; Nie, Z.H.; Wang, M.G.; Wang, Z.L.; Suo, H.L.; Ren, Y.; Wang, Y.D. Large magnetic entropy change and magnetoresistance in a Ni₄₁Co₉Mn₄₀Sn₁₀ magnetic shape memory alloy. *J. Alloys Compd.* **2015**, *647*, 1081–1085. [[CrossRef](#)]
39. Karaca, H.E.; Karaman, I.; Basaran, B.; Ren, Y.; Chumlyakov, Y.I.; Maier, H.J. Magnetic field-induced phase transformation in NiMnCoIn magnetic shape-memory alloys—a new actuation mechanism with large work output. *Adv. Funct. Mater.* **2009**, *19*, 983–998. [[CrossRef](#)]
40. Nayak, A.K.; Suresh, K.G.; Nigam, A.K. Giant inverse magnetocaloric effect near room temperature in Co substituted NiMnSb Heusler alloys. *J. Phys. D Appl. Phys.* **2009**, *42*, 035009. [[CrossRef](#)]
41. Monroe, J.A.; Karaman, I.; Basaran, B.; Ito, W.; Umetsu, R.Y.; Kainuma, R.; Koyama, K.; Chumlyakov, Y.I. Direct measurement of large reversible magnetic-field-induced strain in Ni-Co-Mn-In metamagnetic shape memory alloys. *Acta Mater.* **2012**, *60*, 6883–6891. [[CrossRef](#)]
42. Roca, P.L.; López-García, J.; Sánchez-Alarcosa, V.; Recartea, V.; Rodríguez-Velamazane, J.A.; Pérez-Landazábal, J.I. Room temperature huge magnetocaloric properties in low hysteresis ordered Cu-doped Ni-Mn-In-Co alloys. *J. Alloys Compd.* **2022**, *922*, 166143. [[CrossRef](#)]
43. Recarte, V.; Pérez-Landazábal, J.I.; Sánchez-Alarcos, V.; Zablotskii, V.; Cesari, E.; Kustov, S. Entropy change linked to the martensitic transformation in metamagnetic shape memory alloys. *Acta Mater.* **2012**, *60*, 3168–3175. [[CrossRef](#)]
44. Lázpita, P.; Pérez-Checa, A.; Barandiarán, J.M.; Ammerlaan, A.; Zeitler, U.; Chernenko, V. Suppression of martensitic transformation in Ni-Mn-In metamagnetic shape memory alloy under very strong magnetic field. *J. Alloys Compd.* **2021**, *874*, 159814. [[CrossRef](#)]
45. Salas, D.; Wang, Y.; Duong, T.C.; Attari, V.; Ren, Y.; Chumlyakov, Y.; Arróyave, R.; Karaman, I. Competing interactions between mesoscale length-scales, order-disorder, and martensitic transformation in ferromagnetic shape memory alloys. *Acta Mater.* **2021**, *206*, 116616. [[CrossRef](#)]
46. Salazar-Mejía, C.; Devi, P.; Singh, S.; Felser, C.; Wosnitza, J. Influence of Cr substitution on the reversibility of the magnetocaloric effect in Ni-Cr-Mn-In Heusler alloys. *Phys. Rev. Mater.* **2021**, *5*, 104406. [[CrossRef](#)]
47. Kainuma, R.; Ito, W.; Umetsu, R.Y.; Oikawa, K.; Ishida, K. Magnetic field-induced reverse transformation in B2-type NiCoMnAl shape memory alloys. *Appl. Phys. Lett.* **2008**, *93*, 091906. [[CrossRef](#)]
48. Ahadi, A.; Sun, Q. Effects of grain size on the rate-dependent thermomechanical responses of nanostructured superelastic NiTi. *Acta Mater.* **2014**, *76*, 186–197. [[CrossRef](#)]
49. Omori, T.; Nagasako, M.; Okano, M.; Endo, K.; Kainuma, R. Microstructure and martensitic transformation in the Fe-Mn-Al-Ni shape memory alloy with B2-type coherent fine particles. *Appl. Phys. Lett.* **2012**, *101*, 231907. [[CrossRef](#)]
50. Bhattacharyya, S.; Jinschek, J.R.; Li, J.F.; Viehland, D. Nanoscale precipitates in magnetostrictive Fe_{1-x}Ga_x alloys for 0.1 < x < 0.23. *J. Alloys Compd.* **2010**, *501*, 148–153.
51. Khachatryan, A.G.; Viehland, D. Structurally heterogeneous model of extrinsic magnetostriction for Fe-Ga and similar magnetic alloys: Part I. decomposition and confined displacive transformation. *Metall. Mater. Trans. A* **2007**, *38A*, 2308–2316.
52. Hane, K.F.; Shield, T.W. Microstructure in the cubic to monoclinic transition in titanium-nickel shape memory alloys. *Acta Mater.* **1999**, *47*, 2603–2617. [[CrossRef](#)]
53. Song, Y.T.; Chen, X.; Dabade, V.; Shield, T.W.; James, R.D. Enhanced reversibility and unusual microstructure of a phase-transforming material. *Nature* **2013**, *502*, 85–88. [[CrossRef](#)]
54. Sun, X.M.; Cong, D.Y.; Ren, Y.; Brown, D.E.; Gallington, L.C.; Li, R.G.; Cao, Y.X.; Chen, Z.; Li, S.H.; Nie, Z.H.; et al. Enhanced negative thermal expansion of boron-doped Fe₄₃Mn₂₈Ga_{28.97}B_{0.03} alloy. *J. Alloys Compd.* **2021**, *857*, 157572. [[CrossRef](#)]

Disclaimer/Publisher’s Note: The statements, opinions and data contained in all publications are solely those of the individual author(s) and contributor(s) and not of MDPI and/or the editor(s). MDPI and/or the editor(s) disclaim responsibility for any injury to people or property resulting from any ideas, methods, instructions or products referred to in the content.